S T U D I A G E O L O G I C A P O L O N I C A

Vol. 129, Kraków 2008, pp. 107–130.

Pennsylvanian (Carboniferous) biotas and palaeoenvironments
Edited by A. Kędzior and C. J. Cleal

Monika Agnieszka KUSIAK[1] & Nonna BAKUN-CZUBAROW[2]

Chemistry of monazites as provenance indicator – case study from the Upper Silesia Coal Basin (Poland)[3]

(Figs 1–7; Tabs 1–5)

Abstract. Mineral chemistry and homogeneity, as well as crystal structure and unit cell parameters of detrital monazites isolated from sandstones of the Upper Silesia Coal Basin were studied using electron microprobe analysis (EPMA) and X-ray diffractometry (XRD). Analyzed monazite grains are chemically almost homogenous, only in a very few cases, parts of the grain are enriched in thorium and depleted in yttrium content. Typical feature of monazite from the Poruba Beds is relatively high content of Y (up to 4 wt. % Y_2O_3), what could point to higher temperature of crystallization. Monazite from the Kwaczała Arkose are, on average, richer in huttonite and slightly poorer in cheralite end-members than monazite from the Poruba Beds. Monazite from Kwaczała Arkose reveals the following unit cell parameters: a = 6.794(1) Å, b = 7.008(2) Å, c = 6.479(2) Å, β = 103.82(2)°, whereas for the Poruba Beds monazite these parameters, excluding b-value, are slightly higher: a = 6.804(3) Å, b = 7.002(5) Å, c = 6.488(4) Å, β = 103.85(3)°.

Key words: Upper Silesia Coal Basin, monazite, REE distribution patterns, XRD patterns, unit cell parameters, provenance indicator.

INTRODUCTION

Monazite, is an anhydrous phosphate of rare earth elements (REE), mostly cerium (Ce,La,Th)PO_4, which name comes from Greek μοναξειυ (monazeis), meaning "to be solitary" (Breithaupt, 1829 – after Overstreet, 1967). It was named in allusion to the rare occurrence of this mineral in its first known localities.

Monazite crystals in different types of rocks commonly contain different compositional domains. Generally, such domains represent new monazite grow or re-

1 Institute of Geological Sciences, Polish Academy of Sciences, Kraków Research Centre, ul. Senacka 1, 31-002 Kraków, Poland. E-mail: ndkusiak@cyf-kr.edu.pl

2 Institute of Geological Sciences, Polish Academy of Sciences, ul. Twarda 51/55, 00-818 Warszawa, Poland. E-mail: nbakun@twarda.pan.pl

3 Accepted for publication on February 15, 2008.

crystallization stages during the geological history (Williams & Jercinovic, 2002; Pyle & Spear, 2003; Williams *et al.*, 2007). The presented work is an extensive elaboration on the chemical variability of monazite grains separated from sandstones of the Upper Silesia Coal Basin (USCB). For research there were selected samples from: (1) the Poruba Beds, belonging to Paralic Series, and (2) the Kwaczała Arkose. Monazite from those samples were previously dated using CHIME (Chemical Th-U-total Pb isochron method) by means of electron (Kusiak *et al.*, 2001; Kusiak *et al.*, 2006) and proton (Lekki *et al.*, 2003) microprobes.

Monazite grains were separated using unconventional separation methods (Kusiak & Paszkowski, 1998; Paszkowski *et al.*, 1999), excluding heavy liquids. Previous work on heavy minerals from the Upper Carboniferous sandstones (Turnau-Morawska & Łydka, 1952; Łydka, 1955; Siedlecka & Krysowska, 1962) do not report the occurrence of monazite in those rocks. It can be due to the fact that monazite is not always optically distinguishable from zircon, allanite, xenotime or titanite.

GEOLOGICAL SETTING

The Upper Silesia Coal Basin (USCB) constitutes a large Late Mississippian to Pennsylvanian marine to non-marine sedimentary basin located in southwestern Poland and the northeastern Czech Republic (Fig. 1). The USCB overlies the Moravo-Silesia Zone to the west and the Kraków – Myszków Zone to the north and northeast. To the south, the basin can be traced by subsurface occurrence of coal beds below Miocene deposits and in nappes in the Outer Carpathian Mountains.

The USCB is a remnant of the Carboniferous foreland of the Variscan Orogen (Gradziński, 1982). The basement consists of Precambrian crystalline rocks of the Cadomian Brno – Upper Silesia Massif, overlain by Devonian–Mississippian platform carbonates. The foredeep succession includes flysch sediments, overlain by a coal-bearing shallow-marine to non-marine molasse. The Pennsylvanian coal-bearing rocks of the USCB concordantly overlie older strata (Kotas, 1972). The stratigraphic thickness of the coal-bearing sequence is estimated at around 8000 m and decreases eastwards (Kotas, 1994). Syn- to post-Carboniferous erosion removed part of the succession in the west. Gradziński (1982) described the depocentres of each stratigraphic unit, showing an eastward gradual shift of the maximum subsidence zone, as commonly observed in flexural foredeep basins.

Based on palaeobotanical, palynological and palaeozoological data, the coal-bearing succession is divided into four, informal units that are, in ascending order of stratigraphic age: (1) the Paralic Series (PS) of the Pendleian–Arnsbergian; (2) the Upper Silesia Sandstone Series (USSS) of the Kinderscoutian–Yedonian; (3) the Mudstone Series (MS) of the Langsettian–Duckmantian; and (4) the Cracow Sandstone Series (CSS) of the Bolsovian–Westphalian D (Dembowski, 1972).

The Paralic Series is interpreted as near-shore marine, deltaic, and fluvial in origin (Doktor and Gradziński, 2002). The Štur marine band (XVI) is the lowest member of this series (Namurian A; Kotas, 1995), whereas the base of the overlying

Fig. 1. A simplified map of the Upper Silesia Coal Basin with marked places of the collected samples

USSS is defined at the bottom of coal seam number 510, which represents the onset of on-shore deposition. The PS is characterized by marine, brackish and fresh-water horizons, and is subdivided into the Petřkovice, Hrušov, Jaklovec and Poruba Beds, based on marine and tuffaceous layers (Kotas & Malczyk, 1972). Each of these units is composed of conglomerates, sandstones, siltstones, claystones and phytogenic facies. Conglomerate clasts include sedimentary rocks, phyllites, quartz-chlorite and quartz-mica schists, microgranites, gneisses and granulites (Paszkowski *et al.*, 1995). Sandstones are composed of arkoses, lithic arenites, sublitharenites and subarkoses (Świerczewska, 1995).

The coal-bearing strata are overlain by the Stephanian Kwaczała Arkose. The Kwaczała Arkose lacks of coal seams and has features of the red-bed facies and contains silicified *Dadoxylons* trunks (Rutkowski, 1972). Petrographic data indicate that the arenites are dominated by detritus derived from metamorphic and magmatic rocks (Świerczewska, 1995). Petrological study of clasts in flysch and molasses associations suggests that the crystalline clastic materials were mostly derived from gneisses, granitoids and ryolitic bodies of the Bohemian Massif (Paszkowski *et al.*, 1995).

MONAZITE

Monazite consists mainly of 21–32% Ce_2O_3, 28–35% (La, Nd,...)$_2O_3$, 6–11% ThO_2 and of about 32% P_2O_5, not being described any natural monazite with pure Ce or Nd content. In the crystal structure $[PO_4]^{3-}$ can be substituted by $[SiO_4]^{4-}$ or $[SO_4]^{2-}$ (Ni *et al.*, 1995) and Th for Ce and La (Frondel, 1958). The upper limit of substitution of thorium is not known, but it is estimated in about 30 weight percent of ThO_2 (31.5 wt.%, noticed by Overstreet, 1967), being the total content of thorium in detrital monazite taken as constant. Usually monazite, next to thorium, contains also uranium, but most often only up to 1 weight percent U_3O_8 (Frondel, 1958). Chemical formula for "typical" monazite estimated by Suzuki *et al.* (1994) is $(Ce_{0.41–0.45}La_{0.20–0.23}Nd_{0.15–0.18})[PO_4]$ + other REE < 6 mol % + Y, Th, U, Ca. The chemical formula for monazite from USCB, calculated for average of 85 grains, is $(Ce_{0.55}La_{0.26}Nd_{0.19})PO_4$. The most significant compositional variation in monazite results from solid-solution with huttonite ($ThSiO_4$), by coupled $Th^{4+}Si^{4+}$-$LREE^{3+}P^{5+}$ substitution (Ayres & Harris, 1997). The thorium content is usually fairly constant due to its entering into the monazite crystal structure through the coupled substitutions $Th^{4+}+Si^{4+}\rightarrow REE^{3+}+P^{5+}$, $Th^{4+}+Ca^{2+} \rightarrow 2REE^{3+}$, and $Th^{4+}+2Si^{4+} \rightarrow Ca^{2+}+2P^{5+}$ (Catlos *et al.*, 2002). Monazite from pegmatites has a significantly higher content of the actinides (U, Th) and Ca (Demartin *et al.*, 1991).

Monazite is mainly a transparent, almost colorless mineral, showing a variety of yellowish shades. Nevertheless, Overstreet (1967) reported black monazite due to carbon contamination. In the Upper Silesia Coal Basin, the black monazite occurs in the Jaklovec Beds in "Rydułtowy" coal mine. Such monazite contains elevated sulfur content (Kusiak *et al.*, 2006). Monazite has a high relief with resinous lustre and it appears with a dark rim surrounding its outline (Mange & Maurer, 1992). Its mineralogical structure is positive biaxial, having a $2V\gamma$+6°–9° angle of optical axes. It displays strong birefringence, Δ = 0.045–0.075 (Deer *et al.*, 1993) and its maximum extinction angle ranges between 2° and 7°. As it is common for detrital grains it does not show a complete extinction (Mange & Maurer, 1992). Monazite's hardness fluctuates between 4.9–5.3 at the Mohs scale (Boenigh, 1983) whilst its density [for a pure monazite (Ce,La)PO_4] is 5.15±0.05 g/cm^3 (Frondel, 1958). Chemical changes in composition can cause variation of density within 4.6–5.5 g/cm^3 (Gribble & Hall, 1992), whereby the density increases with increasing thorium content.

Monazite is a monoclinic mineral (prismatic crystal class 2/m) and belongs to the $P2_1/n$ space group. Crystals are mostly plate and often thick tabular on {100} or flattened and elongated along the c-axis or the a-axis (Frondel, 1958). Monazite crystals have often rough, uneven or striated faces due to alteration, showing distinct cleavage on the {100} face and less distinct on the {010} one. Monazite undergoes neither chemical nor structural changes below 1000°C (Frondel, 1958).

There are nine distinct bond distances between the REE and oxygen ions in the monoclinic monazite structure. A regular variation of the REE cation-to-oxygen bond distances is typical for both, monazite and xenotime (Ni *at al.*, 1995). There

are four $LaPO_4$ molecules per Bravais unit-cell. In the $(La_{1-2x}Ac_xCa_x)PO_4$ series, the filling of the Cat^{3+} cation sites by atoms of Th (respectively U) or Ca in the monoclinic structure of $LaPO_4$ is random (Podor, 1995).

In the monazite crystal structure, the larger trivalent cation is coordinated by nine O-atoms in a rather irregular arrangement. These polyhedra link by sharing edges to form chains that extend in the b-direction. The chains are linked in the c-direction by (PO_4) tetrahedra that share edges with polyhedra of adjacent chain to form a layer parallel to (100). These layers stack in the a-direction by sharing edges between the ({REE}O_9) polyhedra to form rather staggered chains that extend in the {101} direction.

Due to the abundance of light rare earth elements, monazite has high magnetic susceptibility (Heaman & Parrish, 1991), having been reported that the most magnetic grains are low in La, Ce and high in Nd, Sm, Gd, Y (Overstreet, 1967).

The isomorphic group of monazite consists of cheralite (Th,Ca,Ce,La,U,Pb)(PO_4,SiO_4) (Bowles *et al.*, 1980) and huttonite Th(SiO_4) (Kucha, 1980; Pabst & Hutton, 1951). The natural thorium orthophosphate end-member, brabantite $CaTh(PO_4)_2$ (Rose, 1980), has been described probably only once. Natural monazite of the intermediate composition between 31.5 and 57 wt% ThO_2 has never been reported (Podor & Cuney, 1997), and brabantite has been discarded as the isomorphic end-member of monazite system (Burke & Ferraris, 2006). Less common in the monazite-group mineral are gasparite (Ce,REE)AsO_4, As-monazite (REE,Y)(PO_4,As_2O_5) (Ondrejka *et al.*, 2007) and Nd-monazite (Nd,Ce)(PO_4,SiO_4) in which Nd is predominant over Ce (Graeser & Schwander, 1987). The distribution of rare earth elements in cheralite is similar to that shown by monazite, especially monazite from granitic pegmatites.

Monazite is a selective mineral for the light rare earth elements (LREE), whereas xenotime incorporates preferentially Y and the heavy rare earth elements (HREE) (Gratz & Heinrich, 1997). LREE minerals from $LaPO_4$ to $GdPO_4$ have monoclinic structure of monazite, but HREE minerals from $TbPO_4$ to $LuPO_4$, and YPO_4 are tetragonal, being isostructural with zircon. This phenomena can explain selective differentiation between HREE and LREE. The exception is Gd, which prefers xenotime crystal structure, but pure $GdPO_4$ crystallizes in monazite structure (Franz *et al.*, 1996; Gratz & Heinrich, 1998). The selectivity of monazite is connected with REE fractionation and growth conditions, and can form the following decreasing order, as monazite from carbonatites contains more La+Ce+Pr than monazite from alkaline rocks and > from quartzite veins > from granitoids > from pegmatites. Monazite from pegmatites are the richest in thorium. Monazite shows relatively steep LREE distribution pattern, a negative Eu-anomaly, and a flat HREE distribution (Franz *et al.*, 1996). The complex zonation pattern in monazite is connected with La and Nd choosing preferentially particular lattice planes (Cressey *et al.*, 1999). The morphology and zonation pattern is a function of REE fractionation. Yttrium zoning may be correlated to Th (and U) zoning, Y zoning is believed to record a history of monazite growth with or without Y-bearing phases (garnet, apatite, xenotime, allanite). Sharp boundaries exist between chemically distinct zones.

This is especially valid for Th, U, and Y, despite high metamorphic grade of some samples (there is poor evidence for diffusional homogenization, possibly except for Y).

Some of monazite grains show metamictisation resulting from the absorption at high doses of ionizing radioactivity from Th and U. In non-changed grains, in UV light, monazite shows no fluorescence (what differs it from zircon) and no or very weak cathodoluminescence. Monazite is not always clearly optically distinguishable from zircon, allanite, xenotime or titanite; third order of its interference colors may resemble epidote, zircon or small titanite grains (Scherrer *et al.*, 2000).

Most often monazite occurs as single grains, in which fluid or gas inclusions are rare. On the other hand, other type of solid inclusions like minute crystals of apatite, biotite, epidote, galena, garnet, hematite, quartz, magnetite, muscovite, rutile, sillimanite are often described. It coexists with ilmenite, rutile, zircon, cassiterite, xenotime, sillimanite and thorite.

Monazite can be used in geological thermobarometry on the basis of presence of HREE in monazite, in spite of selective REE fractionation. The pressure has no significant effect on the partitioning, until it reaches a range of 2 to 5 kbar (Gratz & Heinrich, 1997). The contents of HREE in monazite and those of LREE in xenotime increase with increasing temperature. The ratio of Gd in monazite to Gd in xenotime increases with the temperature of metamorphism from 0.25 for T=500°C to 1.0 for T=1000°C (Gratz & Heinrich, 1998). Monazite retentive nature for Pb, its tendency to grow over a range of P-T, and its unusual behaviour during diagenesis is unstable and, according to the Overstreet (1967), does not reappear until albite-epidote-amphibolite-facies or staurolite-zone conditions) suggest its use as a system capable of recording thermochronological information during prograde metamorphism of a pelite (Akers *et al.*, 1993).

Monazite and xenotime are used as geothermometers, mainly due to the REE partitioning (Gratz & Heinrich, 1997). The LREE are preferentially fractionated into monazite and the HREE into xenotime. Monazite crystals formed at high temperature could contain up to 5% Y_2O_3 (Jonasson *et al.*, 1988). With the increase of temperature, minor HREE (Gd-Yb) content in monazite and LREE (Ce, Nd, Sm) content in xenotime also increase (Andrehs & Heinrich, 1998; Gratz & Heinrich, 1998). The use of monazite composition as geothermometer would be of great value, because it could allow to obtain temperature-time point values on a single mineral grain, what would have wide application in petrogenesis, thermochronology and tectonics.

Because of its ability to accept U and Th in crystal structure, monazite is one of the most radioactive minerals after uraninite, thorianite or thorite. This feature makes monazite a very useful tool for the U/Pb and Sm/Nd isotope geochronology (Parrish & Tirrul, 1989; Noble & Searle, 1995; Hawkins & Bowring, 1999; Vavra & Schaltegger, 1999; Zhu & O'Nions, 1999; Krohe & Wawrzenitz, 2000), and for chemical CHIME dating (Suzuki & Adachi, 1991, 1994; Montel *et al.*, 1996; Braun *et al.*, 1998; Finger & Helmy 1998). Lead produced by U and Th decay, has a place in the mineral structure. Therefore, there is no natural tendency for Pb to be released

from monazite, as could be in the case of zircon (Bosch *et al.*, 2002). Nevertheless, some studies of the diffusion of Pb in monazite indicate that Pb loss may be experienced by crystals during a high-temperature metamorphic event (Suzuki *et al.*, 1994). As a diffusion is a thermally activated process, the amount of Pb diffused in monazite corresponds to the intensity of the metamorphic overprint. According to Crowley and Ghent (1999), the diffusion zones were 18–22 μm thick in monazite grains metamorphosed at 620°C, while they were much thicker (48–58 μm) in grains metamorphosed at 680°C. In hydrothermal experiments, monazite releases or incorporates Pb from a fluid depending on its relative concentrations and the external conditions (Seydoux-Guillaume *et al.*, 2002)

The development of *in situ* (= in thin section) dating techniques, like for example SIMS, LA-ICP-MS or EPMA, makes possible to obtain Th-U, U-Pb or Pb-Pb ages on individual spots in a grain. This allows the age determination on individual chemical zones within a crystal. *In situ* dating of monazite makes possible dating differences between the age of monazite as inclusion in garnet and those in the rock's matrix (Foster, *et al.*, 2000; Catlos, *et al.*, 2002). The same techniques have been applied to date metamorphic events (Parrish, 1990; Dunning *et al.*, 1995; Kalt *et al.*, 2000; Pyle & Spear, 2003), as well as to describe hydrothermal activity, mineralization processes (Corfu & Muir, 1989) and for dating detrital grains (Kusiak *et al.*, 2006). It was thought that the closing temperature for U-Pb in monazite is up to about 725°C (Copeland *et al.*, 1988; Parrish, 1990; Hawkins & Bowring, 1999), being the crystallization age preserved at higher temperature than for the granulite facies (Gebauer & Grunenfelder, 1979; Copeland *et al.*, 1988; Smith & Barreiro, 1989; De Wolf *et al.*, 1993; Suzuki *et al.*, 1994; Bingen & van Breemen, 1998; Vavra *et al.*, 1998; Timmermann *et al.*, 2000). The recent experimental studies (Cherniak *et al.*, 2004) suggest the closing temperature in monazite above 900°C. According to Spear & Pyle (2002), closing temperature above 800°C (up to 850°C) characterizes monazite inclusions in garnets (Montel *et al.*, 2000).

Monazite is a typical detrital mineral because of its physical and chemical stability and is of worldwide occurrence in beach and river sands and placer deposits. Most abundantly it occurs as subhedral to rounded grains, and is often found as tiny (< microns) grains. It tends to concentrate in black sands, because of its relatively high specific gravity, and is found with magnetite, ilmenite, zircon, garnet, rutile and other heavy minerals.

Economically, the most important monazite deposits are beach placers. Monazite is the main ore for the commercial extraction of thorium, and it has also been used as a secondary source of uranium (Boatner, 2002). In crystalline rocks, the chemical and physical aspects of geologic environment affect the presence, amount, and composition of monazite, but in sedimentary rocks these relations are subject to mechanical processes in the environment.

METHODS

Electron Probe MicroAnalysis – EPMA. Monazite were analyzed on a JEOL JXA-8600 superprobe, equipped with three wavelength-dispersive type spectrometers, based in the Saskatchewan University in Saskatoon, Canada. The accelerating voltage was 20 kV, the probe current was about 100 nA, and the effective beam diameter was 2μm. The PET crystal was used to analyze Pb, Th, U, Ca, P and Y, TAP crystal to analyze Si, and LIF crystal to analyze the whole spectrum of REE. The X-ray line, crystal, count time and calibration standards for each element are listed in Tab. 1. Analysed X-ray lines give minimum interferences. The background was measured in half the time on each side of the peak. The chemical composition of the standards used is given in Tab. 2.

X-ray diffraction. X-ray data of two monazite samples were obtained using CGR transmission diffractometer with Bragg-Brentano optics, working in a Debye-Scherrer-Hall geometry with the capillary sample stage. The diffractometer was equipped with curved position-sensitive detector INEL CPS-120 having sample-to-detector distance of 250 mm. The Co $K\alpha_1$ radiation monochromatized with focusing quartz monochromator as well as counting time of 48 hours were applied.

Table 1

Conditions of EMPA analysis for monazites

Element	X-ray line	Crystal	Count time	Calibration standard
Si	Kα	TAP	20 sec	Structure Probe Inc. – quartz (SiO2 – 99.99)
Ca	Kα	PET	20 sec	Smithsonian Durango apatite
P	Kα	PET	20 sec	Smithsonian Durango apatite
La	Lα	LIF	30 sec	Smithsonian synthetic LaPO4
Ce	Lα	LIF	30 sec	Smithsonian synthetic CePO4
Pr	Lβ	LIF	50 sec	Smithsonian synthetic PrPO4
Nd	Lβ	LIF	50 sec	Smithsonian synthetic NdPO4
Sm	Lβ	LIF	50 sec	Smithsonian synthetic SmPO4
Eu	Lβ	LIF	50 sec	Smithsonian synthetic EuPO4
Gd	Lβ	LIF	50 sec	Smithsonian synthetic GdPO4
Dy	Lβ	LIF	50 sec	Smithsonian synthetic DyPO4
Er	Lα	LIF	30 sec	Smithsonian synthetic ErPO4
Yb	Lα	LIF	30 sec	Smithsonian synthetic YbPO4
Lu	Lα	LIF	30 sec	Smithsonian synthetic LuPO4
Y	Lα	PET	100 sec	Smithsonian synthetic YPO4
Th	Mα	PET	100 sec	Structure Probe Inc. Th metal (Th – 99.99)
U	Mβ	PET	200 sec	Structure Probe Inc. U metal (U – 99.99)
Pb	Mβ	PET	200 sec	Structure Probe Inc. crocoite

Table 2

The chemical composition of used standards

Calibration standard	Chemical composition [wt.%]
Smithsonian Durango apatite	SiO_2 – 0.34, CaO – 54.02, Na_2O – 0.23, P_2O_5 – 40.78, REE - 1.43, SO_3 - 0.37, F - 3.53, Cl - 0.41
Smithsonian synthetic $LaPO_4$	La_2O_3 – 59.39, PO_4 – 40.61
Smithsonian synthetic $CePO_4$	Ce_2O_3 – 59.60, PO_4 – 40.40
Smithsonian synthetic $PrPO_4$	Pr_2O_3 – 59.73, PO_4 – 40.27
Smithsonian synthetic $NdPO_4$	Nd_2O_3 – 60.30, PO_4 –39.70
Smithsonian synthetic $SmPO_4$	Sm_2O_3 – 61.28, PO_4 – 38.72
Smithsonian synthetic $EuPO_4$	Eu_2O_3 – 61.54, PO_4 –38.46
Smithsonian synthetic $GdPO_4$	Gd_2O_3 – 62.34, PO_4 –37.66
Smithsonian synthetic $DyPO_4$	Dy_2O_3 – 63.11, PO_4 – 36.89
Smithsonian synthetic $ErPO_4$	Er_2O_3 – 63.78, PO_4 –36.22
Smithsonian synthetic $YbPO_4$	Yb_2O_3 – 64.56, PO_4 –35.44
Smithsonian synthetic $LuPO_4$	Lu_2O_3 – 64.81, PO_4 –35.19
Smithsonian synthetic YPO_4	Y_2O_3 – 48.35, PO_4 – 51.65
Structure Probe Inc. crocoite	PbO – 69.06, Cr_2O_3 –30.94

Up to 5 mg of powdered monazite samples were loaded to Lindemann-glass capillaries with inner diameter of 0.3 mm, filling them up to 8 mm high. Unit-cell parameters were calculated from X-ray powder diffraction data using UCIN software and the standard diffractogram of monazite no 11–0556 from JCPDS–ICDD database.

RESULTS

Analyzed monazite grains show typical features of this mineral with characteristic yellowish shadows. Grains are dominantly well rounded, usually "egg-shaped" or spherical. In spite of being mostly rounded, there are grains with clearly distinguishable faces, what is shown on Fig. 2. Surprisingly, in the investigated sandstone beds, monazite is concentrated not only in the finest fraction (below 0.23 mm) but also is often cumulated in a coarser fraction of 0.23–0.32 mm. Some of the grains contain inclusions of other minerals: quartz, feldspar, pyrite, apatite, zircon and other monazite. Monazite, forming inclusions in other monazite grains usually contain more thorium than it is in the host-mineral.

From both samples ten separated grains were selected for EPMA analyses. Altogether there were 21 spots analysed in each of sets. All points of analyses and chemical compositions are shown on the pictures and in the tables (Fig. 3 with Tab. 3 and Fig. 4 with Tab. 4, for Poruba Beds and Kwaczała Arkose respectively).

Monazite grains from the Poruba Beds contain 2.63–8.03 wt% ThO_2, 0.22–1.06 wt% UO_2, up to 0.2 wt% PbO and 0.32–4.09 wt% Y_2O_3, 0.50–1.94 wt% CaO and

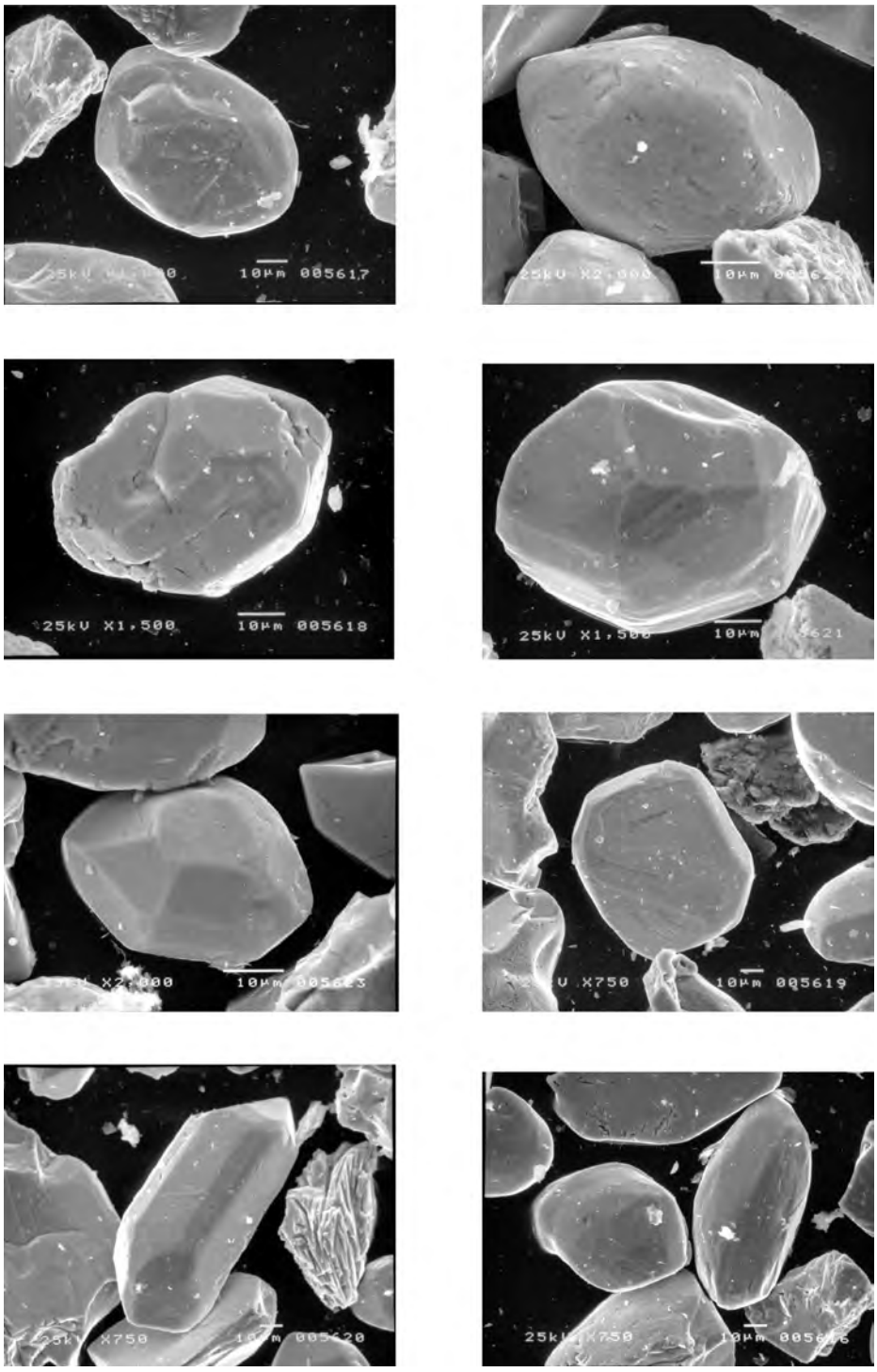

Fig. 2. SEM-EDS images of unpolished monazite grains showing their morfology

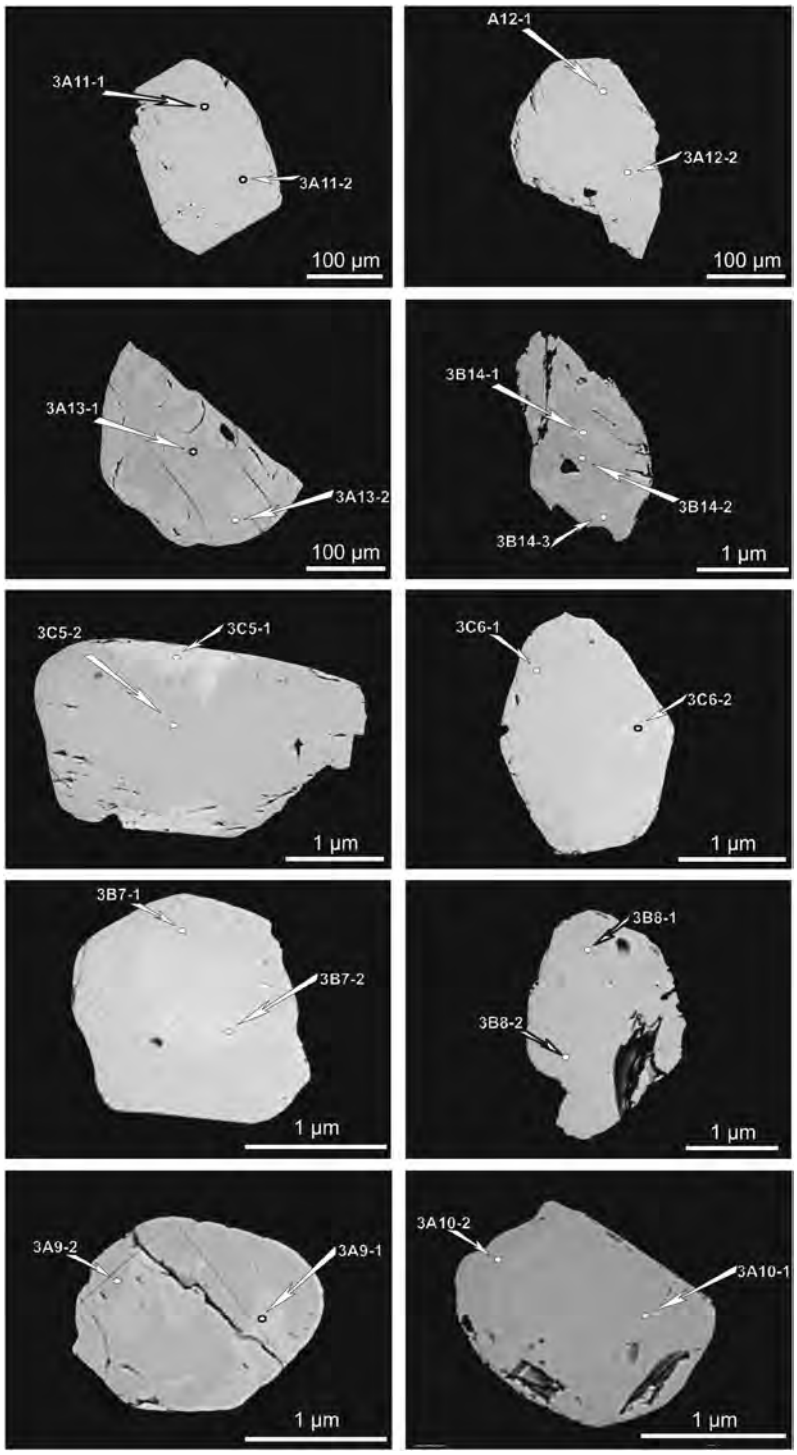

Fig. 3. BSE image of 10 monazite grains from Poruba Beds with marked points of analysis

Table 3

Chemical compositions of monazites from Poruba Beds [wt.%]

Pt#	SiO_2	ThO_2	UO_2	Y_2O_3	La_2O_3	Ce_2O_3	Pr_2O_3	Nd_2O_3	Sm_2O_3	Eu_2O_3	Gd_2O_3	Dy_2O_3	Er_2O_3	Yb_2O_3	Lu_2O_3	CaO	PbO	P_2O_5	Total
3A11-1	0.26	4.19	0.81	2.64	13.13	27.64	2.90	9.21	1.73	0.04	1.37	0.65	0.00	0.00	0.00	1.09	0.00	32.75	98.43
3A11-2	0.29	4.26	0.97	2.64	14.38	27.53	2.92	8.71	1.88	0.06	1.50	0.75	0.01	0.00	0.00	1.08	0.13	33.12	100.24
3A12-1	0.39	3.70	0.54	4.09	12.89	25.68	2.76	10.30	2.04	0.25	1.86	0.71	0.01	0.00	0.00	0.87	0.05	32.16	98.29
3A12-2	0.40	3.38	0.36	2.59	14.15	27.79	2.76	9.58	1.97	0.00	1.67	0.64	0.02	0.05	0.01	0.72	0.00	32.29	98.39
3A13-1	0.85	6.25	0.10	1.83	13.41	27.55	2.90	9.70	1.64	0.13	1.01	0.31	0.08	0.02	0.05	1.94	0.00	30.46	98.23
3A13-2	1.06	6.41	0.19	2.30	12.92	26.24	2.97	9.14	1.71	0.22	0.94	0.42	0.14	0.00	0.00	1.57	0.09	31.36	97.67
3B14-1	0.90	5.81	0.68	0.77	15.26	28.90	2.80	8.90	1.66	0.00	0.72	0.15	0.00	0.00	0.00	0.93	0.07	31.70	99.25
3B14-2	0.32	4.44	0.91	2.62	12.85	27.45	2.33	9.74	2.06	0.04	1.33	0.67	0.00	0.00	0.02	1.18	0.11	31.84	97.91
3B14-3	0.55	6.25	0.41	0.74	13.18	28.39	2.69	9.88	2.14	0.03	1.30	0.21	0.00	0.00	0.05	1.11	0.20	31.69	98.82
3C5-1	0.86	5.47	0.20	0.48	17.98	30.48	3.47	7.64	0.75	0.00	0.19	0.00	0.00	0.00	0.00	0.63	0.00	31.94	100.08
3C5-2	0.94	5.30	0.19	0.32	17.07	31.36	3.21	7.70	0.94	0.00	0.28	0.00	0.00	0.00	0.00	0.50	0.10	31.09	99.00
3C6-1	0.22	2.92	0.29	2.77	13.34	27.64	3.15	9.50	1.81	0.00	1.74	0.58	0.12	0.04	0.05	0.68	0.04	32.48	97.36
3C6-2	0.27	3.91	0.35	3.48	11.93	26.61	3.10	10.08	1.88	0.08	1.97	0.82	0.00	0.01	0.00	0.82	0.15	32.81	98.29
3B7-1	0.35	4.84	0.76	3.27	12.69	25.88	2.47	9.46	1.84	0.14	1.78	0.76	0.00	0.00	0.02	1.11	0.00	32.48	97.86
3B7-2	0.38	5.24	0.77	3.13	12.48	25.81	3.37	9.30	1.93	0.02	1.60	0.83	0.01	0.00	0.00	1.18	0.10	32.48	98.63
3B8-1	0.86	8.03	0.12	0.88	12.86	28.75	2.94	9.84	1.62	0.00	0.97	0.11	0.04	0.00	0.00	1.33	0.12	31.78	100.23
3B8-2	0.78	7.87	0.16	0.73	13.39	27.60	2.82	9.66	1.53	0.16	0.84	0.00	0.00	0.00	0.00	1.26	0.10	31.54	98.44
3A9-1	0.38	5.76	0.44	2.17	14.63	27.12	3.16	9.30	1.77	0.06	0.82	0.38	0.00	0.05	0.07	1.15	0.08	32.36	99.69
3A9-2	0.26	4.47	0.39	2.83	13.71	26.92	3.17	9.26	2.17	0.09	1.56	0.63	0.01	0.02	0.01	1.00	0.07	32.60	99.17
3A10-1	0.33	2.63	0.52	2.06	13.23	28.69	2.82	9.31	2.01	0.42	1.63	0.38	0.00	0.00	0.03	0.66	0.09	32.70	97.51
3A10-2	0.24	3.24	0.72	2.34	13.27	28.16	3.33	9.60	2.30	0.38	1.16	0.65	0.00	0.00	0.00	0.85	0.15	32.85	99.22
max	1.06	8.03	0.97	4.09	17.98	31.36	3.47	10.30	2.30	0.42	1.97	0.83	0.14	0.05	0.07	1.94	0.20	33.12	
min	0.22	2.63	0.10	0.32	11.93	25.68	2.33	7.64	0.75	0.00	0.19	0.00	0.00	0.00	0.00	0.50	0.00	30.46	

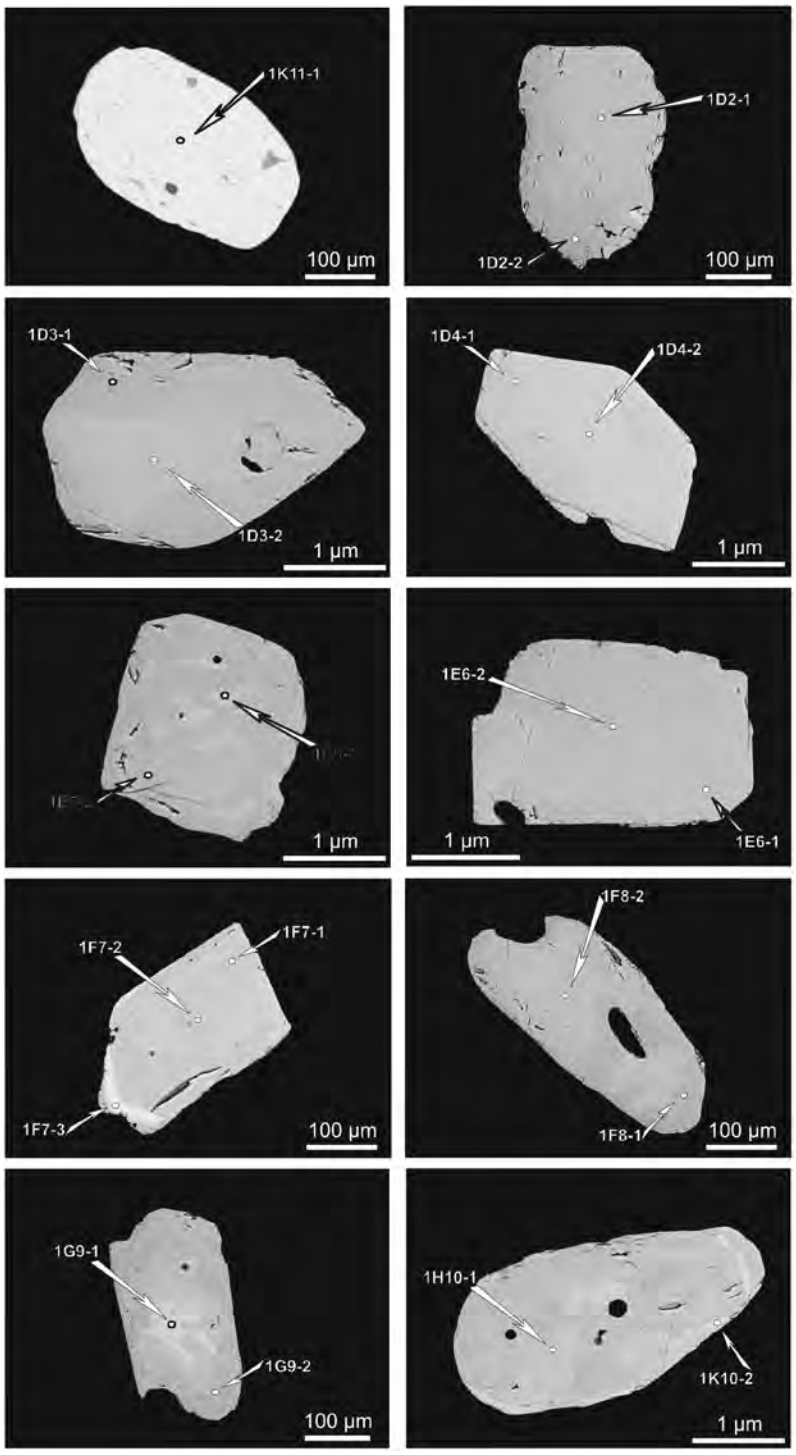

Fig. 4. BSE image of 10 monazite grains from Kwaczała Arkose with marked points of analysis

Table 4

Chemical compositions of monazites from Kwaczała Arkose [wt.%]

Pt#	SiO_2	ThO_2	UO_2	Y_2O_3	La_2O_3	Ce_2O_3	Pr_2O_3	Nd_2O_3	Sm_2O_3	Eu_2O_3	Gd_2O_3	Dy_2O_3	Er_2O_3	Yb_2O_3	Lu_2O_3	CaO	PbO	P_2O_5	Total
1K11-1	0.20	4.31	0.86	2.82	14.33	27.66	3.05	8.64	1.49	0.00	1.33	0.58	0.14	0.01	0.06	1.04	0.09	32.68	99.29
1K11-2	0.24	4.34	0.59	3.17	13.16	27.05	2.95	9.07	1.84	0.11	1.49	0.57	0.03	0.01	0.00	0.96	0.13	32.42	98.13
1D2-1	2.55	10.31	0.17	0.91	16.22	28.85	2.68	6.68	1.01	0.13	0.33	0.00	0.00	0.03	0.03	0.61	0.16	28.65	99.32
1D2-2	1.96	8.11	0.10	1.82	15.72	27.66	2.55	7.55	1.25	0.00	0.78	0.28	0.00	0.07	0.00	0.68	0.05	30.00	98.58
1D3-1	0.87	5.83	1.09	3.28	11.46	25.60	2.63	9.17	1.67	0.23	1.73	0.71	0.00	0.00	0.03	1.03	0.17	31.82	97.32
1D3-2	0.83	6.06	1.20	3.25	12.29	25.66	2.47	9.47	1.87	0.18	1.48	0.68	0.04	0.08	0.03	1.14	0.16	32.20	99.11
1E4-1	0.29	4.29	0.40	3.16	13.44	27.15	3.19	9.23	1.91	0.00	1.23	0.56	0.13	0.00	0.00	0.97	0.11	33.06	99.13
1E4-2	0.26	4.41	0.47	3.51	12.82	26.94	3.10	8.99	1.74	0.00	1.37	0.70	0.02	0.00	0.10	0.92	0.12	32.05	97.50
1E5-1	0.33	4.39	0.49	1.41	13.91	28.15	3.07	9.54	1.70	0.16	1.30	0.31	0.00	0.00	0.02	0.95	0.08	32.59	98.39
1E5-2	0.46	5.00	0.28	0.94	14.30	28.12	2.91	10.46	1.74	0.00	1.29	0.24	0.00	0.00	0.04	1.02	0.04	33.07	99.91
1E6-1	0.25	4.61	0.90	3.13	12.44	25.08	2.74	10.18	2.25	0.11	1.63	0.78	0.00	0.00	0.00	1.19	0.13	33.07	98.48
1E6-2	0.25	4.46	0.74	3.04	13.12	26.17	3.35	10.12	2.33	0.23	1.80	0.73	0.00	0.00	0.07	1.14	0.14	32.98	100.67
1F7-1	1.86	7.38	0.62	0.51	14.52	31.04	3.55	9.21	1.39	0.02	0.59	0.00	0.00	0.05	0.06	0.55	0.07	30.21	101.64
1F7-2	1.84	7.23	0.64	0.39	15.27	29.04	2.61	8.56	0.96	0.00	0.35	0.00	0.03	0.05	0.00	0.51	0.12	29.06	96.67
1F7-3	3.38	14.35	0.42	0.67	13.51	26.90	2.84	8.39	1.31	0.00	0.41	0.00	0.00	0.00	0.00	0.46	0.11	26.72	99.47
1F8-1	0.23	4.28	0.51	3.20	13.02	26.81	3.37	9.74	2.01	0.22	1.49	0.61	0.08	0.00	0.00	1.04	0.00	32.63	99.24
1F8-2	0.39	4.77	0.52	1.30	14.11	29.03	3.18	10.23	1.58	0.07	1.29	0.27	0.00	0.00	0.03	0.97	0.07	32.11	99.94
1G9-1	0.59	6.97	0.86	1.31	14.32	26.91	2.90	7.50	1.31	0.07	0.82	0.29	0.00	0.00	0.00	1.41	0.14	32.09	97.50
1G9-2	0.24	4.63	0.34	3.64	12.11	27.20	3.46	9.28	1.80	0.00	1.82	0.79	0.00	0.03	0.07	1.11	0.14	33.62	100.28
1K10-1	1.05	2.90	0.04	0.67	17.07	33.86	3.32	8.47	0.99	0.10	0.29	0.06	0.00	0.00	0.00	0.38	0.00	31.44	100.62
1K10-2	1.90	8.65	0.13	0.66	15.68	29.81	2.42	8.05	1.01	0.00	0.34	0.00	0.00	0.00	0.00	0.56	0.13	29.88	99.21
max	3.38	14.35	1.20	3.64	17.07	33.86	3.55	10.46	2.33	0.23	1.82	0.79	0.14	0.08	0.10	1.41	0.17	33.62	
min	0.20	2.90	0.04	0.39	11.46	25.08	2.42	6.68	0.96	0.00	0.29	0.00	0.00	0.00	0.00	0.38	0.00	26.72	

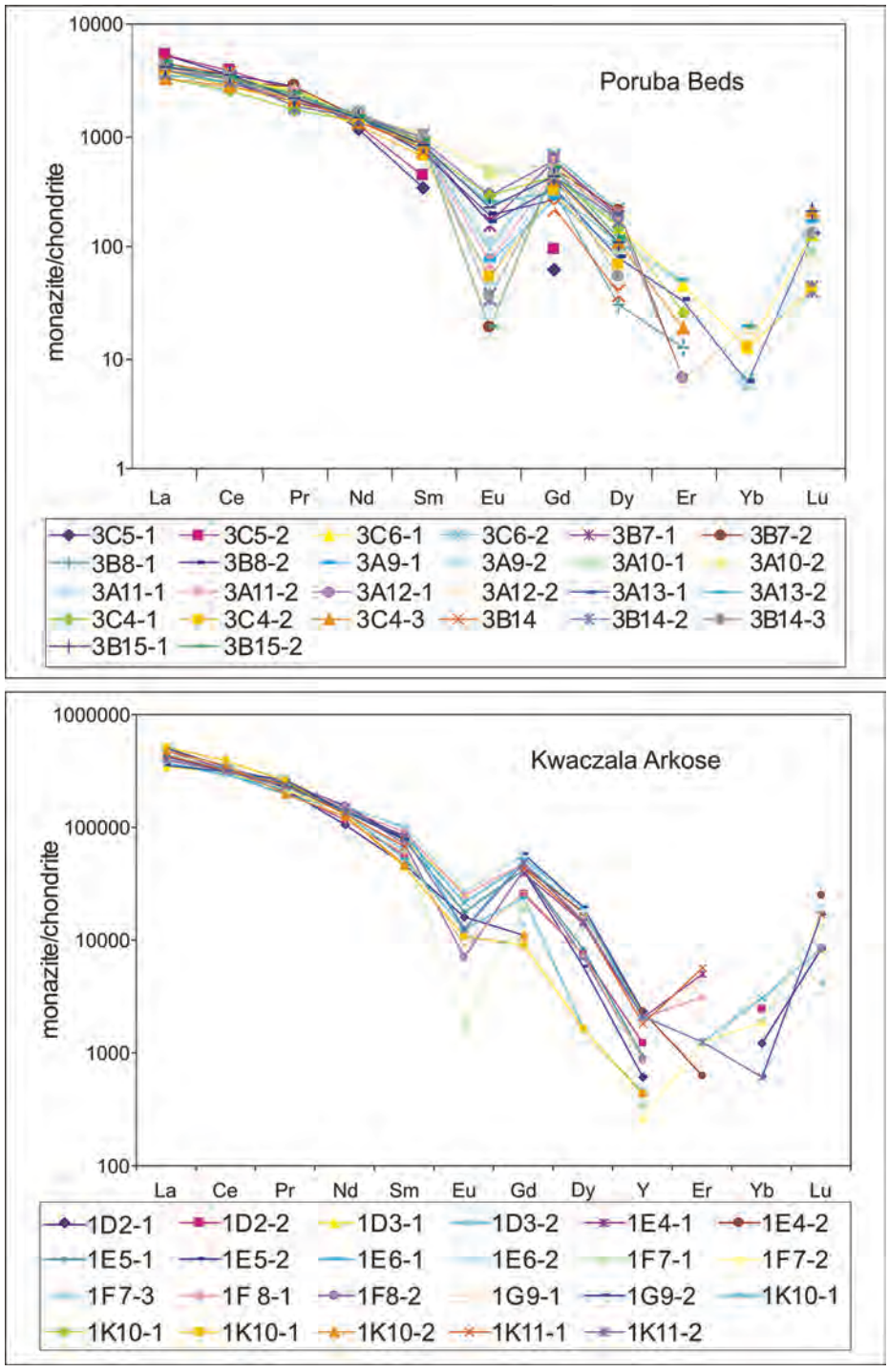

Fig. 5. Chondrite normalized REE + Y distribution of monazite in samples from Poruba Beds and Kwaczała Arkose

Table 5

X-ray data for powdered monazites and unit cell parameters

			Monazite from Kwaczała Arkose			Monazite from Poruba Beds			JC PDS-ICDD 11-0556	
h	k	l	d_{obs}	d_{cal}	I	dobs	dcal	I	d	I
-1	0	1	5.204	5.218	5	5.221	5.227	7	5.2	13
1	1	0	4.804	4.804	8	4.808	4.805	6	4.82	7
0	1	1	4.684	4.681	11	4.688	4.683	18	4.66	18
-1	1	1	4.183	4.185	25	4.186	4.188	21	4.17	25
1	0	1	4.076	4.091	6	4.109	4.095	10	4.08	9
0	2	0	3.500	3.504	18	3.504	6.501	20	3.51	25
2	0	0	3.298	3.299	56	3.304	3.303	55	3.30	50
1	2	0	3.092	3.095	100	3.094	3.094	100	3.09	100
2	1	0	2.930	2.985	14	2.985	2.987	14	2.99	18
-1	1	2	2.869	2.870	62	2.873	2.874	73	2.87	70
-2	0	2	2.606	2.609	14	2.608	2.613	17	2.61	18
1	1	2	2.441	2.444	16	2.445	2.446	19	2.44	18
2	2	0							2.40	5
-1	2	2							2.34	5
-3	0	1	2.250	2.250	4	2.250	2.254	2	2.25	3
0	3	1	2.189	2.190	24	2.191	2.189	29	2.19	18
-1	0	3	2.152	2.152	18				2.15	25
-1	3	1				2.127	2.131	23	2.13	25
1	3	1							2.02	3
2	1	2	1.966	1.964	29	1.968	1.965	34	1.961	25
3	0	1							1.933	7
-3	2	1	1.896	1.893	15	1.896	1.895	17	1.895	13
1	0	3	1.873	1.873	34	1.875	1.876	38	1.870	18
3	2	0	1.863	1.863	18	1.864	1.864	16	1.859	18
0	2	3	1.800	1.799	9	1.800	1.801	8	1.797	9
2	2	2	1.766	1.767	11	1.766	1.768	16	1.762	18
1	3	2	1.740	1.740	26	1.741	1.740	29	1.737	25
-3	1	3				1.692	1.691	13	1.689	13
1	2	3	1.651	1.652	5	1.653	1.653	8	1.645	7
-3	3	1							1.623	7
-3	3	0							1.600	7
2	3	2							1.535	13
2	4	1							1.463	5
-3	1	4	1.423	1.424	3				1.423	3
4	2	1	1.386	1.386	3				1.386	3
0	5	1							1.368	5
1	2	4							1.339	9
2	4	2							1.329	9
-4	0	4	1.305	1.304	4				1.307	3
-1	5	2	1.280	1.280	14				1.280	6

Table 5 continued

			Monazite from Kwaczała Arkose			Monazite from Poruba Beds			JC PDS-ICDD 11-0556	
h	k	l	d_{obs}	d_{cal}	I	dobs	dcal	I	d	I
-5	0	3							1.261	2
4	2	2	1.248	1.248	7				1.245	3
5	0	1	1.234	1.234	20	1.235	1.235	18	1.233	9
-3	5	1							1.189	3
0	6	0	1.168	1.168	12				1.168	6
2	5	2							1.153	3
-2	5	3							1.145	2
1	5	3							1.121	4
6	0	0	1.099	1.100	15				1.099	4
6	1	0							1.086	2
-6	1	3							1.074	2
1	6	2							1.064	3
0	0	6							1.046	4
0	1	6							1.034	2
-4	3	5							1.025	2
-6	3	2							1.014	2
3	6	1							0.9998	2
1	6	3							0.9899	2
4	5	2							0.9659	2
-5	3	5							0.9523	3
2	0	6							0.9343	3
-4	3	6							0.9181	3
7	0	1							0.9012	3
-6	4	4							0.8831	2
-1	6	5							0.8667	3
-7	4	1							0.8462	3
2	8	1							0.8320	2
1	7	4							0.8238	3
-1	4	7							0.8134	2
-2	1	8							0.8038	2
-1	1	8							0.7966	3
a (Å)			6.794 ± 0.001			6.804 ± 0.003			6.796	
b (Å)			7.008 ± 0.002			7.002 ± 0.005			7.006	
c (Å)			6.479 ± 0.002			6.488 ± 0.004			6.466	
β (°)			103.82 ± 0.02			103.85 ± 0.03			103.95	

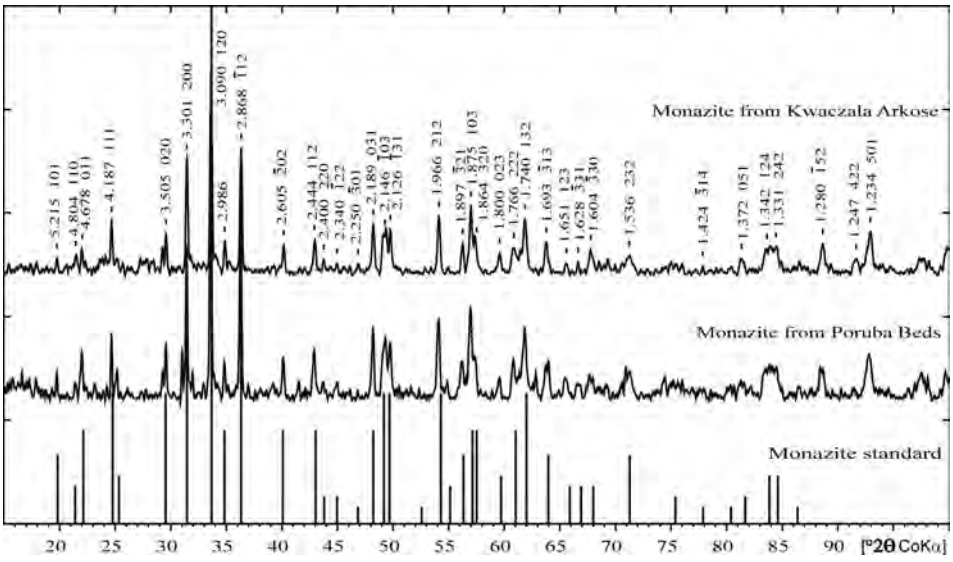

Fig. 6. X-ray diffraction patterns of the analyzed monazites

0.22–1.06 wt% SiO_2. Despite of the patchy pattern on few monazite grains, their chemical composition is quite homogeneous, showing no zoning. Brighter spots show higher Th content, but the differences are not very big between brighter and darker spots (see Fig. 3, analysis 3B14).

Chondrite normalized diagram for REE+Y data is presented on the Fig. 5-top. Yttrium is plotted between Dy and Ho on the basis of its ionic radius. The calculated chemical formula of monazite from the Poruba Beds is $(Ce_{0.36–0.45}La_{0.17–0.25}Nd_{0.10–0.14})(PO_4)$+other REE, with average of $(Ce_{0.39}La_{0.19}Nd_{0.13})(PO_4)$+other REE.

The general lack of zoning may reflect the growth of grains during a single reaction or as a result of recrystallisation of older monazite material. Recrystallisation features are visible on grain 3C5 (spot of 3C5-1, Fig. 3). Some of euhedral monazite grains from the Poruba Beds show slight evidence of abrasion, which may be an indicator of igneous source rock.

Monazite grains from the Kwaczała Arkose display slightly different chemical composition showing some depletion in light REE and enrichment in heavier ones and thorium. The chemical composition is as follows: 2.90 – 14.35 wt% ThO_2, 0.04 – 1.20 wt% UO_2, up to 0.17 wt% PbO and 0.39 – 3.64 wt% Y_2O_3, 0.38 – 1.41 wt% CaO and 0.20–3.28 wt% SiO_2. Those grains display some visible zonation, e.g., sector zoning (Fig. 4 – grain 1D3) or so-called "patchy" (Zhu & O'Nions, 1999) zonation (e.g., Fig. 4 – grain 1E5). Some monazite have margins highly enriched in Th (Fig. 4 – grain 1F7). In this sample recrystallization features on the grains are visible as well (Fig. 4 – grain 1G9). The calculated chemical formulae of monazite from the Kwaczała Arkose differs slightly from those of the Poruba Beds $(Ce_{0.37–0.47}La_{0.16–0.23}Nd_{0.09–0.14})[PO_4]$ + other REE, with average of $(Ce_{0.39}La_{0.20}Nd_{0.12})[PO_4]$ + other REE, being enriched in light REE.

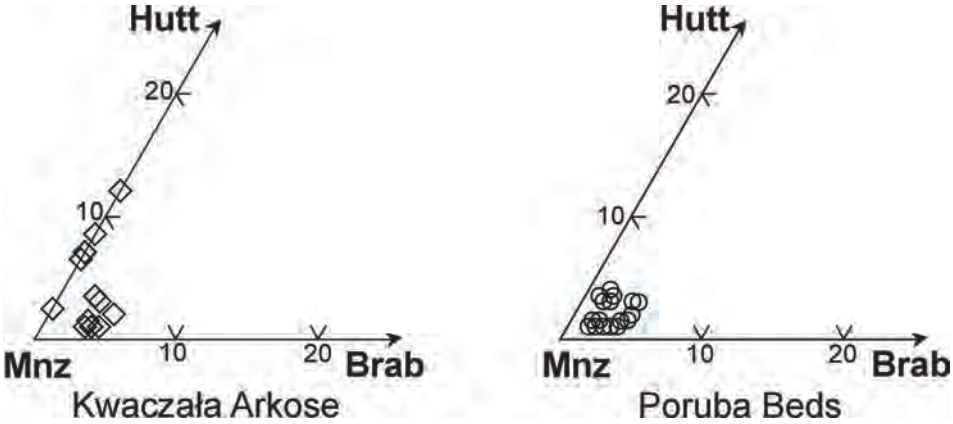

Fig. 7. Contents of huttonite (Hutt) and brabantite (Brab) end members in monazites (Mnz) from analyzed samples

The zoning observed in BSE images is reflected by chemical composition of monazite. Dark zones have lower Th (+Ca+Si) and higher Y (+HREE) contents when compared to the light ones. There is a negative correlation between Th (+Ca+Si) and Y (+HREE) and between Th and LREE, what reflects the typical coupled substitution: $Th^{4+}+Ca^{2+}=2REE^{3+}$ and $Th^{4+}+Si^{4+}=LREE^{3+}+P^{5+}$. Yttrium, which is positively correlated with heavy REE, substitutes REE, and typically behaves similarly to the HREE. There is no systematic correlation between U and Th.

Monazite grains from the Kwaczała Arkose and Poruba Beds do not differ significantly, neither in X-ray diffraction patterns nor in the unit cell parameters, but the PB monazite's values are higher. Transmission diffraction patterns of the powdered monazite are given on Fig. 6, whereas X-ray data together with unit cell parameters are presented in Tab. 5. The Poruba Beds monazite grains show the following unit cell parameters: a = 6.804(3) Å, b = 7.002(5) Å, c = 6.488(4) Å, β = 103.85(3)°, while the parameters for monazite from the Kwaczała Arkose, excluding b-value, are slightly lower: a = 6.794(1) Å, b = 7.008(2) Å, c = 6.479(2) Å, β = 103.82(2)°.

CONCLUSIONS

The provenance of the rocks forming the Upper Carboniferous Coal Basin succession were discussed previously (Paszkowski *et al.*, 1995; Kusiak *et al.*, 2006). This study is the next step for supplementing our knowledge.

1. A characteristic feature of the analyzed monazites is relatively high content of yttrium, especially for grains from the Poruba Beds, which have up to 4 wt % Y_2O_3, what could be caused by relatively high temperature of their crystallization. Apart from high-Y monazite, there also occurs a high thorium population (up to 27.9 wt % of ThO_2) among these detrital minerals from the geological units in question.

2. Monazite grains from the Kwaczała Arkose are, on an average, richer in huttonite (3.6 mol.%) than monazites from the Poruba Beds (2.1 mol.%), which, on the other hand, are slightly richer in brabantite (2.9 mol.%) than the Kwaczała Arkose monazites (2.3 mol.% – Fig. 7). One can also observe a relatively strong negative correlation between (REE + P) and (Th + Si) as well as between LREE (La+Ce+Nd) and (Th + Ca), what can be explained by the presence of monazite–huttonite and monazite–brabantite solid solutions, respectively. In the analyzed monazites from Poruba Beds, there is a positive correlation between lanthanum and actinides (Th+U), whereas for the monazite grains from the Kwaczala Arkose, this correlation is negative.

3. On the base of our observation we can assume that both units could be formed from different types of rocks. Monazites from the Poruba Beds display the feature of grains coming from high grade metamorphic rocks. On the other hand, the monazites which occur in the Kwaczała Arkose, are rather igneous like. Our conclusion is not an ultimate one. It is still possible, that the amount of analyzed detrital grains is not representative enough, or that source rocks could be mixture of different types of rocks. The strontium content in monazite, which is indicating high metamorphic facies for growing of monazite (Kusiak *et al.*, 2008), was not measured for this study. The present-day studies of monazite grains from different types of crystalline rocks, are conducted due to clear up the provenance problem.

Acknowledgments

We thank Dr Mariusz Paszkowski for inspiring ideas, Prof. Kazuhiro Suzuki and Dr Daniel J. Dunkley for discussions, Dr Artur Kędzior and Mrs Danuta Kusy for help during graphic work, Prof. Yuanming Pan for the assistance in the laboratory work and helpful discussions. Prof. Wojciech Narębski is thanked for reviewing the paper. The authors are grateful to M.Sc. Michał Kuźniarski for recording the X-ray transmission diffractograms of monazite and to M.Sc. Dorota Grabska for interpretation of the monazite XRD patterns as well as for calculation of the unit cell parameters. M.A. Kusiak is a fellow of the Foundation for Polish Sciences (Homing Fellowship).

REFERENCES

Andrehs, G. & Heinrich, W., 1998. Experimental determination of REE distrubutions between monazite and xenotime: potential for temperature-calibrated geochronology. *Chemical Geology*, 149: 83–96.

Akers, W. T., Grove, M., Harrison, T. M. & Ryerson, F. J., 1993. The instability of rhabdophane and its unimportance in monazite paragenesis. *Chemical Geology*, 110: 169–176.

Ayres, M. & Harris, N., 1997. REE fractionation and Nd-isotope disequilibrium during crustal anatexis: constraints from Himalayan leucogranites. *Chemical Geology*, 139: 249–269.

Bingen, B. & van Breemen, O., 1998. U-Pb monazite ages in amphibolite- to granulite-facies orthogneiss reflect hydrous mineral breakdown reactions; Sveconorwegian province of SW Norway. *Contributions to Mineralogy and Petrology*, 132: 336–353.

Boatner, L. A., 2002. Synthesis, structure, and properties of monazite, pretulite, and xenotime. *In*: M. J. Kohn, J. Rakovan & J. M. Hughes (eds), Phosphates: Geochemical, Geobiological, and Materials Importance. *Reviews in Mineralogy and Geochemistry*, 48: 87–121.

Boenigh, W., 1983. Schwermineralanalyse. *Enke*, 158 pp.

Bosch, D., Hammor, D., Bruguier, O., Caby, R. & Luck, J. M., 2002. Monazite "in situ" $^{207}Pb/^{206}Pb$ geochronology using a small geometry high-resolution ion probe: Application to Archaean and

Proterozoic rocks. *Chemical Geology*, 184: 151–165.
Bowles, J. F. W., Jobbins, E. A. & Young, B. R., 1980. A re-examination of cheralite. *Mineralogical Magazine*, 43: 885–888.
Braun, I., Montel, J. M. & Nicollet, C., 1998. Electron microprobe dating of monazite from high-grade gneisses and pegmatites of the Kerala Khondalite Belt, southern India. *Chemical Geology*, 146: 65–85.
Burke E. A. J. & Ferraris, G. 2006. New minerals approved in 2006 nomenclature modifications approved in 2006 by the commission on new minerals and mineral names. *International Mineralogical Association*.
Catlos, E. J., Gilley, L. D. & Harrison, T. M., 2002. Interpretation of monazite ages obtained via *in situ* analysis. *Chemical Geology*, 188: 193–215.
Cherniak, D. J., Watson, E. B., Grove, M. & Harrison, T. M., 2004. Pb diffusion in monazite: A combined RBS/SIMS study. *Geochemica et Cosmochimica Acta*, 68: 829–840.
Copeland, P., Parrish, R. R. & Harrison, T. M., 1988. Identification of inherited radiogenic Pb in monazite and its implications for U-Pb system. *Nature*, 333: 760–763.
Corfu, F. & Muir, T. L., 1989. The Hemlo-Heron Bay greenstone belt and Hemlo Au-Mo deposit, Superior Province, Ontario, Canada. Timing of metamorphism, alteration and Au mineralization from titanite, rutile, and monazite U-Pb geochronology. *Chemical Geology*, 79: 201–223.
Cressey, G., Wall, F. & Cressey, B. A., 1999. Differential REE uptake by sector growth of monazite. *Mineralogical Magazine*, 63: 813–828.
Crowley, J. L. & Ghent, E. D., 1999. An electron microprobe study of the U-Th-Pb systematics of metamorphosed monazite: the role of Pb diffusion versus overgrowth and recrystallization. *Chemical Geology*, 157: 285–302.
Deer, W. A., Howie, R. A. & Zussman, J., 1993. *An introduction to the rock-forming minerals.* Longman Scientific & Technical: 337–346.
Demartin, F., Pilati, T., DielIa, V., Donzelli, S. & Gramacciolli, C. M., 1991. Alpine monazite: further data. *Canadian Mineralogist*, 29: 61–67.
Dembowski, Z., 1972. Ogólne dane o Górnośląskim Zagłębiu Węglowym (General information on the Upper Silesian Coal Basin – in Polish, English summary). *Prace Instytutu Geologicznego* (Warszawa), 61: 9–22.
De Wolf, C. P., Belshaw, N. & O'Nions, R. K., 1993. A metamorphic history from micron-scale $^{207}Pb/^{206}Pb$ chronometry of Archean monazite. *Earth and Planetary Science Letters*, 120: 207–220.
Doktor, M. & Gradziński, R., 2002. Sedymentacja osadów węglonośnej sukcesji Górnośląskiego Zagłębia Węglowego (Sedimentation of coal-bearing succession in the Upper Silesia Coal Basin – in Polish, English summary). *In*: Kožušniková A. (ed.), The 5th Czech-Polish Conference "Geology of the Upper Silesian Basin", *Documenta Geonica,* Ostrava: 35–40.
Dunning, G. R., Macdonald, A. S. & BARR, A. S., 1995. Zircon and monazite U-Pb dating of the Doi Inthanon core complex, northern Thailand: implications for extension within the Indosinian Orogen. *Tectonophysics*, 251: 197–213.
Finger, F. & Helmy, H. M., 1998. Composition and total-Pb model ages of monazite from high-grade paragneisses in the Abu Swayel area, southern Eastern Desert, Egypt. *Mineralogy and Petrology*, 62: 269–289.
Foster, G., Kinny, P., Vance, D., Prince, C. & Harris, N., 2000. The significance of monazite U-Th-Pb age data in metamorphic assemblages; a combined study of monazite and garnet chronometry. *Earth and Planetary Science Letters*, 181: 327–340.
Franz, G., Andrehs, G. & Rhede, D., 1996. Crystal chemistry of monazite and xenotime from Saxothuringian – Moldanubian metapelites, NE Bavaria, Germany. *European Journal of Mineralogy*, 8: 1097–1118.
Frondel, C., 1958. Systematic mineralogy of uranium and thorium. *U.S. Geological Survey Bulletin*, 1064: 150–160.
Gebauer, D. & Grunenfelder, M., 1979. *U-Th-Pb dating of minerals*. *In*: E. Jager & J. C. Hunziker (eds), Lectures in isotope geology. Springer Verlag NY: 105–131.

Gradziński, R., 1982. Explanatory notes to the lithotectonic molasse profile of the Upper Silesian Basin (Upper Carboniferous–Lower Permian). *Veröffentlichungen des Zentralinstitut für Physik der Erde Ad W DDR*, Potsdam: 225–135.

Graeser, S. & Schwander, H., 1987. Gasparite-(Ce) and monazite-(Nd): two new minerals to the monazite group from the Alps. *Schweizerische Mineralogische und Petrographische Mitteilungen*, 67: 103–113.

Gratz, R. & Heinrich, W., 1997. Monazite-xenotime thermobarometry: Experimental calibration of the miscibility gap in the binary system $CePO_4$-YPO_4. *American Mineralogist*, 82: 772–780.

Gratz, R. & Heinrich, W., 1998. Monazite-xenotime thermometry. III. Experimental calibration of the partitioning of gadolinium between monazite and xenotime. *European Journal of Mineralogy*, 10: 579–588.

Gribble, C. D. & Hall, A. J., 1992. Optical mineralogy, Principles and practise. *UCL Press, London*, 187pp.

Hawkins, D. P. & Bowring, S. A., 1999. U-Pb monazite, xenotime and titanite geochronological constraints on the prograde to post-peak metamorphic thermal history of Paleoproterozoic migmatites from the Gran Canyon, Arizona. *Contributions to Mineralogy and Petrology*, 134: 150–169.

Heaman, L. & Parrish, R., 1991. U-Pb geochronology of accessory minerals. *In*: L. Heaman & J. N. Ludden (eds), Short course handbook on applications of radiogenic isotope systems to problems in geology. *Mineralogical Association of Canada*, 19: 59–102.

Jonasson, R. G., Bancroft, G. M. & Boatner, L. A., 1988. Surface reactions of synthetic, end-member analogues of monazite, xenotime and rhabdophane, and evolution of natural waters. *Geochimica et Cosmochimica Acta*, 52: 767–770.

Kalt, A., Corfu, F. & Wijbrans, J. R., 2000. Time calibration of a P-T path from a Variscan high-temperature low-pressure metamorphic complex (Bayerische Wald, Germany), and the detection of inherited monazite. *Contributions to Mineralogy and Petrology*, 138: 143–163.

Kotas, A., 1972. Osady morskie karbonu górnego i ich przejście w utwory produktywne Górnośląskiego Zagłębia Węglowego (Marine sediments of tye Upper Carboniferous in the Upper Silesia Coal Basin– in Polish, English summary). *Prace Instytutu Geologicznego* (Warszawa), 61: 279–328.

Kotas, A., 1994. Coal deposits and coal resources. *Prace Państwowego Instytutu Geologicznego* (Warszawa), 142: 18–26.

Kotas, A., 1995. Lithostratigraphy and sedimentologic-paleogeographic development, Moravian-Silesian-Cracovian region, Upper Silesian Coal Basin. *In*: Zdanowski A. & Żakowa H. (eds), The Carboniferous System in Poland. *Prace Państwowego Instytutu Geologicznego* (Warszawa), 148: 124–134.

Kotas, A. & Malczyk, W., 1972. Seria paraliczna piętra namuru dolnego Górnośląskiego Zagłębia Węglowego (The Paralic Series of the Lower Namurian Stage of the Upper Silesian Coal Basin – in Polish, English summary). *Prace Instytutu Geologicznego* (Warszawa), 61: 329–425.

Krohe, A. & Wawrzenitz, A. P., 2000. Domainal variations of U-Pb monazite ages and Rb-Sr whole-rock dates in polymetamorphic paragneisses (KTB Drill Core, Germany): influence of strain and deformation mechanisms on isotope systems. *Journal of Metamorphic Geology*, 18: 271–291.

Kucha, H., 1980. Continuity in the monazite-huttonite series. *Mineralogical Magazine*, 43: 1031–1034.

Kusiak, M. & Paszkowski, M., 1998. Wydzielanie minerałów ciężkich za pomocą separatora magnetohydrostatycznego (New methods of separation using magnetohydrostatic separator – in Polish). *Przegląd Geologiczny* (Warszawa), 46: 674–675.

Kusiak, M., Suzuki, K. & Paszkowski, M., 2001. Preliminary report of CHIME dating on detrital monazite grains from the Namurian Poruba Beds and the Stephanian Kwaczala Arkose in the Upper Silesia Coal Basin, Poland. *Journal of Earth and Planetary Sciences, Nagoya University*, 48: 15–41.

Kusiak, M. A., Kędzior, A., Paszkowski, M., Suzuki, K., González-Álvarez, I., Wajsprych, B. &

Doktor, M., 2006. Provenance implications of Th-U-Pb electron microprobe ages from detrital monazite in the Carboniferous Upper Silesia Coal Basin, Poland. *Lithos*, 88: 56–71.

Kusiak, M. A., Suzuki, K., Dunkley, D. J., Lekki, J., Bakun-Czubarow N., Paszkowski, M. & Budzyń, B., 2008. EPMA and PIXE dating of granulites from Gierałtów, Bohemian Massif, Poland. *Gondwana Research*. doi: 10.1016/j.gr.2008.02.05

Lekki J., Lebed, S., Paszkowski, M. L., Kusiak, M., Vogt, J., Hajduk, R., Polak, W., Potempa, A., Stachura, Z. & Styczeń, J., 2003. Age determination of monazites using the new experimental chamber of the Cracow proton microprobe. *Nuclear Instruments and Methods in Physics Research* B: 210: 472–477.

Łydka, K., 1955. Studia petrograficzne nad permo-karbonem krakowskim. (Petrographic studies concerning the Permo-Carboniferous of the Cracow Region – in Polish, English summary). *Biuletyn Instytutu Geologicznego* (Warszawa), 97, 1: 205–227.

Mange, M. A. & Mauer, H. F. W., 1992. *Heavy minerals in colour*. Chapman & Hall, London.

Montel, J. M., Foret, S., Veschambre, M., Nicollet, Ch. & Provost, A., 1996. Electron microprobe dating of monazite. *Chemical Geology*, 131: 37–53.

Montel, J. M., Kornprobst, J. & Vielzeuf, D., 2000. Preservation of old U-Th-Pb ages in shielded monazite: example from the Beni Bousera Hercynian kinzigites (Morocco). *Journal of Metamorphic Geology*, 18: 335–342.

Ni, Y., Hughes, J. M. & Mariano, A. N., 1995. Crystal chemistry of the monazite and xenotime structures. *The American Mineralogist*, 80: 1–26.

Noble, S. R. & Searle, M. P., 1995. Age of crustal melting and leucogranite formation from U-Pb zircon and monazite dating in the western Himalaya, Zanskar, India. *Geology*, 23,12: 1135–1138.

Ondrejka, M., Uher, P., Pršek, J. & Ozdín, D., 2007. Arsenian monazite-(Ce) and xenotime-(Y), REE arsenates and carbonates from the Tisovec-Rejkovo rhyolite, Western Carphatians, Slovakia: Composition and substitutions in the (REE,Y)XO4 system (X=P, As, Si, Nb, S). *Lithos,* 95: 116–129.

Overstreet, W. C., 1967. The geological occurrence of monazite. *U.S. Geological Survey Professional Paper*, 530: 327 pp.

Pabst, A. & Hutton, C. O., 1951. Huttonite, a new thorium silicate. *The American Mineralogist*, 36: 60–69.

Parrish, R. R., 1990. U-Pb dating of monazite and its application to geological problems. *Canadian Journal of Earth Sciences*, 27: 1431–1450.

Parrish, R. R. & Tirrul, R., 1989. U-Pb age of the Baltoro granite, northwest Himalaya, and implications for monazite U-Pb systematics. *Geology*, 17: 1076–1079.

Paszkowski, M., Jachowicz, M., Michalik, M., Teller, L., Uchman, A. & Urbanek, Z., 1995. Composition, age and provenance of gravel-sized clasts from the Upper Carboniferous of the Upper Silesia Coal Basin. *Studia Geologica Polonica*, 108: 45–127.

Paszkowski, M., Kusiak, M. & Banaś, M., 1999. Nowe, niekonwencjonalne metody w preparatyce minerałów akcesorycznych (Novel, unconventional methods of accessory mineral processing – in Polish, English summary). *In*: Kožušniková A. (ed.), The 4 th Czech-Polish Conference about Carboniferous Sedimentology. *Documenta Geonica*, Ostrava: 147–150.

Podor, R., 1995. Raman spectra of the actinide-bearing monazites. *European Journal of Mineralogy*: 1353–1360.

Podor, R. & Cuney, M., 1997. Experimental study of Th-bearing $LaPO_4$ (780°C, 200 mpa): Implications for monazite and actinide orthophosphate stability. *The American Mineralogist*, 82: 765–771.

Pyle, J. M & Spear, F. S., 2003. Four generations of accessory-phases growth in low-pressure migmatites from SW New Hampshire. *The American Mineralogist*, 88: 338–351.

Rose, D. (1980) Brabantite, CaTh[PO4]2, a new mineral of the monazite group. *Neues Jahrbuch fur Mineralogie, Monatshefte*, 6: 247–257.

Rutkowski, J., 1972. Osady stefanu Górnośląskiego Zagłębia Węglowego (The Stephanian sediments of the Upper Silesian Coal Basin. – in Polish, English summary). *Prace Instytutu Geologicznego* (Warszawa), 61: 539–556.

Scherrer, N. C., Engi, M., Gnos, E., Jacob, V. & Liechti, A., 2000. Monazite analysis; from sample preparation to microprobe age dating and REE quantification. *Schweizerische Mineralogische und Petrographische Mitteilungen*, 80: 93–105.

Seydoux-Guillaume, A. M., Paquette, J. L., Wiedenbeck, M., Montel, J. M. & Heinrich, W., 2002. Experimental resetting of the U-Th-Pb systems in monazite. *Chemical Geology*, 191: 165–181.

Siedlecka, A. & Krysowska, M., 1962. Badania nad genezą i rozprzestrzenieniem piaskowców karniowickich w północnym obrzeżeniu rowu krzeszowickiego (Karniowice sandstone – their provenance on the north of Krzeszowice trough – in Polish). *Rocznik Polskiego Towarzystwa Geologicznego* (Kraków), 32, 3: 371–398.

Smith, H. A. & Barreiro, B., 1989. Using monazite to date staurolite-grade metamorphism in a multiply metamorphosed region: West Central Maine. *Geological Society of America, Abstracts & Program*, 21 A: 285.

Spear, F. S. & Pyle, J. M., 2002. Apatite, monazite, and xenotime in metamorphic rocks. *In*: Kohn M. J., Rakovan J. & J. M. Hughes (eds), Phosphates: geochemical, geobiological, and materials importance. *Reviews in Mineralogy and Geochemistry*, 48: 293–335.

Suzuki, K. & Adachi, M., 1991. Precambrian provenance and Silurian metamorphism of the Tsubonosawa paragneiss in the South Kitakami terrane, Northeast Japan, revealed by the chemical Th-U-total Pb isochron ages of monazite, zircon and xenotime. *Geochemical Journal*, 25: 357–376.

Suzuki, K. & Adachi, M., 1994. Middle Precambrian detrital monazite and zircon the Hide gneiss on Oki-Dogo Island, Japan: their origin and implications for the correlation of basement gneiss of Southwest Japan and Korea. *Tectonophysics*, 235: 277–292.

Suzuki, K., Adachi, M. & Kajizuka, I., 1994. Electron microprobe observations of Pb diffusion in metamorphosed detrital monazites. *Earth and Planetary Science Letters*, 128: 391–405.

Świerczewska, A., 1995. Composition and provenance of Carboniferous sandstones from the Upper Silesia Coal Basin (Poland). *Studia Geologica Polonica*, 108: 27–43.

Timmermann, H., Parrish, R. R., Noble, S. R. & Kryza, R., 2000. New U-Pb monazite and zircon data from the Sudetes Mountains in SW Poland: evidence for a single-cycle Variscan orogeny. *Journal of the Geological Society of London*, 157: 265–268.

Turnau-Morawska, M. & Łydka, K., 1952. Studia petrograficzne nad arkozą kwaczalską (Petrographic analyses on the Kwaczała Arkose – in Polish). *Rocznik Polskiego Towarzystwa Geologicznego* (Kraków), 22 (4): 473–494.

Vavra, G. & Schaltegger, U., 1999. Post-granulite facies monazite growth and rejuvenation during Permian to Lower Jurassic thermal and fluid events in the Ivrea Zone (Southern Alps). *Contributions to Mineralogy and Petrology,* 134: 405–414.

Vavra, G., Reinhardt, Todt, W. & Pidgeon, R. T., 1998. Dating the exhumation of a hot core complex (Saxonian Granulite Massif) – old prejudices and new perspectives of U-Pb dating zircons and monazites. *Freiberger Forschungsheft*, 471: 226–228.

Williams, M. L. & Jercinovic, M. J., 2002. Microprobe monazite geochronology: putting absolute time into microstructural analyses. *Journal of Structural Geology*, 24: 1013–1028.

Williams, M. L., Jercinovic, M. J. & Hetherington, C. J., 2007. Microprobe monazite geochronology: understanding geologic processes by integrating composition and chronology. *Annual Review of Earth and Planetary Sciences,* 35: 137–175.

Zhu, X. K. & O'Nions, R. K., 1999. Zonation of monazite in metamorphic rocks and its implications for high temperature thermochronology: a case study from the Lewisian terrain. *Earth and Planetary Science Letters*, 171, 2: 209–220.